Int. J. Anal. Appl. (2025), 23:152

International Journal of Analysis and Applications

Heat and Mass Transfer Analysis of Magnetized Micropolar Nanofluid Flow With Soret and Dufour Effects: Triple Solutions

Khuram Rafique[1], Gamal Elkahlout[2,*], Abdulkafi Mohammed Saeed[3]

[1]*Department of Mathematics, University of Sialkot, Sialkot 51310, Pakistan*
[2]*Faculty of Business Studies, Arab Open University, Riyadh, Saudi Arabia*
[3]*Department of Mathematics, College of Science, Qassim University, Saudi Arabia*
**Corresponding author:* g.elkahlout@arabou.edu.sa

Abstract: Energy and mass transfer play a major role in several engineering and technological processes, such as air conditioning, mechanical power collectors, food processing, refrigeration, and heat exchangers. This research aims to investigate the radiative flow of an incompressible hydromagnetic micropolar nanofluid by incorporating Soret and Dufour effects. The flow partial differential equations of this study are developed using the boundary layer approximation. The modeled equations are then transformed into nonlinear ordinary differential equations by applying the appropriate transformation. The MATLAB package that comes with BVP4C is used to establish the numerical solutions for this investigation. In addition, a comparison of the outcomes is presented with previously published material. The comparison shows that, in a particular case, our current results resemble the previous results very well. It is observed that temperature distribution shows an increasing behavior against the increment in Soret and Dufour impacts.

1. Introduction

Nanofluids have gained popularity with the development of nanotechnology. Nanofluid has almost better stability than the microfluid because here nanometer-sized particles are suspended in the base fluid. Its convective heat transmission ratio and thermophysical characteristics are better than those of the base liquid alone. Because of this, scientists have used this particular heat transfer fluid in practical applications.

Received Mar. 31, 2025

2020 Mathematics Subject Classification. 76R10.

Key words and phrases. micropolar nanofluid; MHD; Soret and Dufour effect; stretching/shrinking surface; stability analysis; heat and mass transfer; radiative flow; BVP4C MATLAB.

https://doi.org/10.28924/2291-8639-23-2025-152

ISSN: 2291-8639

Nanofluid are utilized in various practical applications including solar collectors, solar thermal energy storage, heat pipes vehicle radiators, refrigeration systems, electronics cooling etc. The main aim of nanofluid technology is to improve the heat transmission rate and thermal properties of the regular liquid. The small size of the nano particles permits them to persevere in liquid phases for months or even for years without sedimentation.

According to Choi [1], a mixture base fluid with nanoparticles is characterized as a "nanofluid." Bouchireb et al., [2] investigated the energy transmission of nanoliquid flow between a convergent divergent channel analytically and numerically. Recently Rafique et al., [3] numerically investigated the nanofluid flow on a rotatory disk by incorporating chemical reaction impact. Furthermore, Ali et al., [4] discussed thermal analysis of nanoliquid flow over a sphere by incorporating Newtonian heating. They concluded that the magnetic impact reduces the flow speed of the liquid. Alotaibi et al., [5] investigated the nanoliquid flow between two discs with the impact of magnetic field numerically.

In addition, Lemouedda et al., [6] considered ternary nanoparticles in the numerical treatment of hybrid nanoliquid rotatory flow. The effect of nanofluid stability on thermal efficiency has been investigated by Cacua et al. [7]. Al Faqih et al., [8] studied the micro-rotational effects on the flow of nanoliquid through a numerical technique by considering inclination impact. Prasad et al. [9] studied energy and mass transfer analysis for the MHD flow of nanofluid with radiations effect.

In energy and mass transmission phenomenon Soret and Dufour impacts play a key role because of their practical applications viewpoint. The Soret effect, also referred to as thermal diffusion, happens when a mass flux is caused by temperature differences. Whereas the Dufour effect, also referred to as the diffusion thermal effect, develops when variations in concentration result in an energy flux. Many applications of the Soret and Dufour effects are present such as the separation of isotopes, heat transfer and chemical separation, petroleum reservoirs, geothermal energy and industrial/chemical processes where they affect mass transfer and heat processes.

The impact of the Soret and Dufour effects on MHD flow over an exponential stretching sheet has been studied by Seema Tinker et al., [10]. Soret and Dufour's influences on mass and heat transfer for magnetohydrodynamic boundary layer flow across a vertical sheet has been explored by Srinivasa et al., [11]. The two-dimensional flow of magnetohydrodynamics over a vertical permeable sheet with Soret and Dufour effect investigated by Vedavathi et al., [12].

Soret and Dufour effects controlling the flow of a nanofluid across a horizontal extending sheet has been investigated by Rasool et al., [13]. The impacts of Soret and Dufour on MHD mixed convection over non-linear stretching/shrinking surfaces were studied by Pal et al. [14]. Rafique et al., [15] calculated the effects of thermophoretic diffusion and Brownian movement on micropolar nanofluid flow with Soret and Dufour impacts through a sloped surface. The impacts of Soret and Dufour on a flow across an infinite vertical plate in a permeable medium have been investigated by Kumar et al., [16].

Magnetohydrodynamics (MHD) is a fundamental theory that describes the interaction between electrically conducting fluids and magnetic fields. MHD is a combination of electromagnetic and fluid mechanics concepts that are used to explain the movement of these conducting fluids and the relationships between their magnetic and electric fields. Numerous fields have found use for it, such as astrophysics, fusion energy, geophysics, space weather, plasma physics, and material processing etc. MHD plays a vital role in advancing our knowledge of plasmas and their behavior in different environments.

The word MHD was first presented by Alfvén [17]. MHD Mixed Convection Flow in Hybrid Nanofluid at Three-Dimensional Stagnation Point has been studied by Nurul Amira Zainal et al. [18]. Investigation on the magnetohydrodynamics flow of a micropolar liquid at the stagnation point on a vertical surface has been observed by Ishak et al. [19]. A study on the effects of mass movement and heat generation on magnetohydrodynamics flow over an inclined vertical surface was proposed by Reddy [20]. Magnetohydrodynamics micropolar fluid flow with chemical reaction to a stagnation point over a vertical plate has been numerically studied by Baag et al. [21].

The prime objective of this research is to analyze the hydromagnetic micropolar nanoliquid flow on an extending/contracting surface by utilizing Buongiorno model. In view of the available literature no study has been conducted on the magnetohydrodynamics boundary layer flow on a vertical stretching/shrinking surface under the impacts of Soret and Dufour. To fill this lack of knowledge, the current study has been conducted.

Additionally, studying the Soret and Dufour impacts could find uses in cooling electronic devices, plastic sheet production, nuclear reactors, polymer manufacture and ceramics. In addition, radiation impacts play a vital role in many technological systems need high temperatures, such as the design of solar power devices, spaceship engines and exploration of space missions. Stability analysis has been carried out to find a stable and feasible solution.

2. Problem Formulation

A steady 2-D boundary layer flow of Micropolar nanofluid flow over a non-linear vertical stretching/shrinking surface along with the impacts of Soret and Dufour are considered. The stretching/shrinking sheet is assumed to have non-linear velocity in the form of $u_w(x) = ax^m$, a variable surface temperature $T_w(x) = T_\infty + bx^{2m-1}$, and concentration $C_w(x) = C_\infty + cx^{2m-1}$, where a, b, c are constants. The temperature T and concentration C at the wall take constant values T_w and C_w. As y tends to infinity, the temperature and concentration reach their ambient values T_∞ and C_∞. The set of boundary equations for micropolar nanofluid flow can be expressed in the following way by applying the boundary layer estimates and the previously stated suppositions.

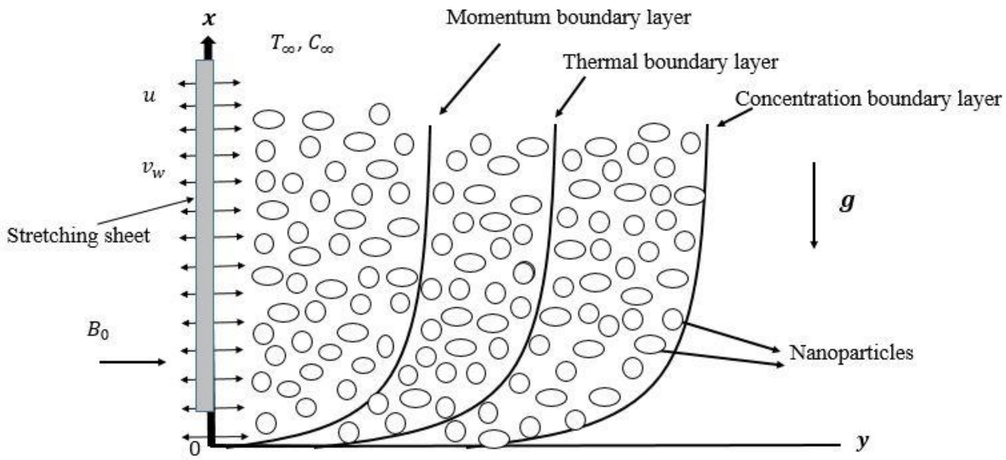

Figure 1: Flow structure with coordinate system

The flow equations for the study under investigation in view of [22-23] are:

$$\frac{\partial u}{\partial x}+\frac{\partial v}{\partial y}=0 \quad (1)$$

$$\left(u\frac{\partial u}{\partial x}+v\frac{\partial u}{\partial y}\right)=(\mu+k)\frac{\partial^2 u}{\partial y^2}+k\frac{\partial N}{\partial y}-\sigma B^2 u+\rho g[\,\beta_T(T-T_\infty)+\ \beta_C(C-C_\infty)] \quad (2)$$

$$u\frac{\partial N}{\partial x}+v\frac{\partial N}{\partial y}=\ \frac{1}{\rho_j}\left[\gamma\frac{\partial^2 N}{\partial y^2}-k\left(2N+\frac{\partial u}{\partial y}\right)\right] \quad (3)$$

$$u\frac{\partial T}{\partial x}+v\frac{\partial T}{\partial y}=\left(\alpha+\frac{16\sigma^* {T_\infty}^3}{3k^*\rho C_p}\right)\frac{\partial^2 T}{\partial y^2}+\ \tau_w\left[D_B\frac{\partial C}{\partial y}\frac{\partial T}{\partial y}+\frac{D_T}{T_\infty}\left(\frac{\partial T}{\partial y}\right)^2\right]-\frac{D_m K_T}{C_s C_p}\frac{\partial^2 C}{\partial y^2} \quad (4)$$

$$u\frac{\partial C}{\partial x}+v\frac{\partial C}{\partial y}=\ D_B\frac{\partial^2 C}{\partial y^2}+\frac{D_T}{T_\infty}\frac{\partial^2 T}{\partial y^2}+\frac{D_m K_T}{T_m}\frac{\partial^2 T}{\partial y^2} \quad (5)$$

Subject to boundary conditions

$$v=v_w\,;u=\lambda u_w(x)\,;N=\ -n\frac{\partial u}{\partial y}\,;T=\ T_w;C=\ C_w \qquad at\ y=0$$
$$u\to 0;v\to 0\,;N\to 0\,;T\to T_\infty\,;C\to C_\infty \qquad as\ y\to\infty \quad (6)$$

Where u and v represents the velocity coefficients along the x-axis and y-axis, respectively. While, ρ,k,j,N,v,γ are density, vortex viscosity, micro-inertia density, angular velocity, kinematic viscosity, spin gradient viscosity, respectively. K^*,σ^* are mean absorption factor, and Stefan-Boltzmann constant respectively. D_m,D_B,D_T,T_m,K_T shows the mass diffusivity, Brownian motion, thermophoresis diffusion, fluid mean temperature, thermal diffusion ratio parameter. $u_w(x)=ax^m$ is a non-linear stretching/shrinking velocity of surface and λ is stretching/shrinking factor where $\lambda<0$ denotes a surface that is shrinking while $\lambda>0$ denotes a surface that is expanding and β is the velocity slip factor. Similarity solutions can be identified by applying the following similarity variables.

$$u = ax^m f', \quad v = -\sqrt{\frac{(m+1)\nu a}{2x^{m+1}}}\, x^m f - yf' \,\frac{ax^{m-1}}{2}(m-1), \quad \eta = y\sqrt{\frac{(m+1)ax^{m-1}}{2\nu}}$$

$$N = \ ax^m \sqrt{\frac{a(m+1)x^{m-1}}{2\nu}}\ h(\eta)\,, \qquad \theta(\eta) = \frac{(T-T_\infty)}{(T_w-T_\infty)}, \tag{7}$$

The following ordinary differential equations are generated by applying similarity transformation to equations (1) – (5).

$$(1+K)f''' + Kh' + ff'' + \left(\frac{2}{m+1}\right)(Gr\,\theta + Gc\,\phi) - \left(\frac{2m}{m+1}\right)f'^2 - \left(\frac{2M}{m+1}\right)f' = 0 \tag{8}$$

$$\left(1+\frac{K}{2}\right)h'' + fh' - \left(\frac{3m-1}{m+1}\right)hf' - \left(\frac{2K}{m+1}\right)(2h + f'') = 0 \tag{9}$$

$$\frac{1}{Pr}\left(1+\frac{4}{3}Rd\right)\theta'' + \ Nb\,\theta'\phi' + Nt\,\theta'^2 + \ \theta' f - Df\,\phi'' = 0 \tag{10}$$

$$\phi'' + \frac{Nt}{Nb}\theta'' + Sr\,Sc\,\theta'' + \phi' f\,Sc = 0 \tag{11}$$

Here primes represents the differentiation with respect to η. $\alpha = \frac{k}{\rho C_p}$ depicts thermal diffusivity parameter. $K = \frac{k}{\nu}$ is a micropolar material parameter. $Pr = \frac{\nu}{\alpha}$ denotes a Prandtl number, $Sc = \frac{\nu}{D_B}$ represents Schmidt number.

Table 1: General factors and their values

Magnetic factor	$M = \dfrac{\sigma B_0^2}{\rho a}$
Brownian motion factor	$Nb = \dfrac{\tau_w D_B(C_w - C_\infty)}{\nu}$
Thermophoresis diffusion factor	$Nt = \dfrac{\tau_w D_T(T_w - T_\infty)}{\nu T_\infty}$
Thermal radiation factor	$Rd = \dfrac{4\sigma^* T_\infty^3}{kK^*}$
Soret factor	$Sr = \dfrac{D_m K_T}{T_m \nu}\dfrac{(T_w - T_\infty)}{(C_w - C_\infty)}$
Dufour factor	$Df = \dfrac{D_m K_T}{\nu C_s C_p}\dfrac{(C_w - C_\infty)}{(T_w - T_\infty)}$
Buoyancy parameter,	$Gr = \dfrac{Gr_x}{Re_x^2}$
Solutal buoyancy parameter	$Gc = \dfrac{Gc_x}{Re_x^2}$

The associative boundary conditions are changed into:

$$f(0) = f_w,\ f'(0) = \lambda,\ h(\eta) = -nf''(\eta),\ \theta(\eta) = 1,\ \phi(\eta) = 1;$$

$$f'(\eta) \to 0\,, \quad h(\eta) \to 0\,, \quad \theta(0) \to 0\,, \quad \phi(0) \to 0 \quad as\ \eta \to \infty \tag{12}$$

In which $v_w = -\sqrt{\frac{a\nu(m+1)}{2}}\ x^{(\frac{m-1}{2})}$ is the suction factor, $f_w > 0$ for suction.

For the current problem, Nusselt, Sherwood number, and skin friction are given as follows:

$$Nu_x = \frac{xq_w}{k(T_w - T_\infty)}, Sh_x = \frac{xq_m}{D_B(C_w - C_\infty)}, C_f = \frac{\tau_w}{u_{w^2}\rho} \tag{13}$$

where,

$$q_w = -\left(k + \frac{16\sigma^* T_\infty^3}{3k^*}\right)\frac{\partial T}{\partial y}, \quad q_m = -D_B\frac{\partial C}{\partial y}, \quad \text{and} \quad \tau_w = (\mu + k)\frac{\partial u}{\partial y} + kN \tag{14}$$

The relevant skin friction factor value is $C_{fx} = (1 + (1 - m)K)f''(0)$, decreased Nusselt number $-\theta'(0)$, and the decreased Sherwood number is $-\phi'$ are described as

$$-\theta'(0) = \frac{Nu_x}{\left(1+\frac{4}{3}Rd\right)\sqrt{\frac{m+1}{2}Re_x}}, \quad -\phi'(0) = \frac{Sh_x}{\sqrt{\frac{m+1}{2}Re_x}}, \quad C_{fx}(0) = C_f\sqrt{\frac{2}{m+1}Re_x}, \ \text{and} \quad Re_x = \frac{u_w x}{\nu} \tag{15}$$

3. Stability Analysis

Stability analysis is an established method used to generate several solutions. The existence of triple solutions is shown by the computational analysis of equations (8) – (11) with boundary conditions (12). To identify the stable and practically possible solution, a stability analysis must be carried out. The first solution to first satisfy the boundary condition is always verified as the feasible and stable solution by performing the stability analysis. Firstly, a new time dependent variable τ must be introduced in order to transform governing equations (2) – (5) into an unsteady form.

$$\rho\left(\frac{\partial u}{\partial t} + u\frac{\partial u}{\partial x} + v\frac{\partial u}{\partial y}\right) = (\mu + k)\frac{\partial^2 u}{\partial y^2} + k\frac{\partial N}{\partial y} - \sigma B^2 u + \rho g[\,\beta_T(T - T_\infty) + \beta_C(C - C_\infty)] \tag{16}$$

$$\left(\frac{\partial N}{\partial t} + u\frac{\partial N}{\partial x} + v\frac{\partial N}{\partial y}\right) = \frac{1}{\rho_j}\left[\gamma\frac{\partial^2 N}{\partial y^2} - k\left(2N + \frac{\partial u}{\partial y}\right)\right] \tag{17}$$

$$\left(\frac{\partial T}{\partial t} + u\frac{\partial T}{\partial x} + v\frac{\partial T}{\partial y}\right) = \left(\alpha + \frac{16\sigma^* {T_\infty}^3}{3k^*\rho C_p}\right)\frac{\partial^2 T}{\partial y^2} + \tau_w\left[D_B\frac{\partial C}{\partial y}\frac{\partial T}{\partial y} + \frac{D_T}{T_\infty}\left(\frac{\partial T}{\partial y}\right)^2\right] - \frac{D_m K_T}{C_s C_p}\frac{\partial^2 C}{\partial y^2} \tag{18}$$

$$\left(\frac{\partial C}{\partial t} + u\frac{\partial C}{\partial x} + v\frac{\partial C}{\partial y}\right) = D_B\frac{\partial^2 C}{\partial y^2} + \frac{D_T}{T_\infty}\frac{\partial^2 T}{\partial y^2} + \frac{D_m K_T}{T_m}\frac{\partial^2 T}{\partial y^2} \tag{19}$$

The following are the new similar parameters that have been presented:

$$u = ax^m\frac{\partial f(\eta,\tau)}{\partial \eta}, \quad v = -\sqrt{\frac{(m+1)\nu a}{2x^{m+1}}}\,x^m f(\eta,\tau) - y\frac{\partial f(\eta,\tau)}{\partial \eta}\frac{ax^{m-1}}{2}(m-1), \ \eta = y\sqrt{\frac{(m+1)ax^{m-1}}{2\nu}}$$

$$\tau = ax^{m-1}t, \ N = ax^m\sqrt{\frac{a(m+1)x^{m-1}}{2\nu}}\,h(\eta,\ \tau), \quad \theta(\eta,\ \tau) = \frac{(T - T_\infty)}{(T_w - T_\infty)}, \quad \phi(\eta,\ \tau) = \frac{(C - C_\infty)}{(C_w - C_\infty)} \tag{20}$$

Equations (16) - (19) are used to obtain it by using equation (20).

$$(1 + K)\frac{\partial^3 f}{\partial \eta^3} + K\frac{\partial h}{\partial \eta} + f\frac{\partial^2 f}{\partial \eta^2} + \frac{2}{m+1}(Gr\,\theta + Gc\,\phi) - \frac{2}{m+1}\frac{\partial^2 f}{\partial \eta \partial \tau} - \frac{2m}{m+1}\left(\frac{\partial f}{\partial \eta}\right)^2 - \frac{2M}{m+1}\frac{\partial f}{\partial \eta} = 0 \tag{21}$$

$$\left(1 + \frac{K}{2}\right)\frac{\partial^2 h}{\partial \eta^2} + f\frac{\partial h}{\partial \tau} - \left(\frac{3m-1}{m+1}\right)h\frac{\partial f}{\partial \eta} - \frac{2K}{m+1}\left(2h + \frac{\partial^2 f}{\partial \eta^2}\right) - \frac{2}{m+1}\frac{\partial h}{\partial \tau} = 0 \tag{22}$$

$$\frac{1}{Pr}\left(1+\frac{4}{3}\,Rd\right)\frac{\partial^2\theta}{\partial\eta^2}+Nb\frac{\partial\theta}{\partial\eta}\frac{\partial\phi}{\partial\eta}+Nt(\frac{\partial\theta}{\partial\eta})^2-\frac{2}{(m+1)}\frac{\partial\theta}{\partial\tau}+f\frac{\partial\theta}{\partial\eta}-Df\,\frac{\partial^2\phi}{\partial\eta^2}=0 \tag{23}$$

$$\frac{\partial^2\phi}{\partial\eta^2}+\frac{\partial\phi}{\partial\eta}f\,Sc+\frac{Nt}{Nb}\,\frac{\partial^2\theta}{\partial\eta^2}-\frac{2}{m+1}\frac{\partial\phi}{\partial\tau}Sc+Sr\,Sc\,\frac{\partial^2\theta}{\partial\eta^2}=0 \tag{24}$$

Subjected to boundary conditions

$$f(0,\tau\,)=f_w,\,\frac{\partial f(0,\tau)}{\partial\eta}=\lambda,\;h(0,\tau)=-n\frac{\partial^2 f(0,\tau)}{\partial\eta^2},\;\theta(0,\tau)=1,\;\phi(0,\tau)=1$$

$$\frac{\partial f(\eta,\tau)}{\partial\eta}\rightarrow 0\,,h(\eta,\tau)\rightarrow 0\,,\theta(\eta,\tau)\rightarrow 0\,,\phi(\eta,\tau)\rightarrow 0 \qquad as\;\eta\rightarrow\infty \tag{25}$$

The perturbation function's goal is to investigate any possible disturbances in the solutions.

$$f(\eta)=f_0(\eta),\;h(\eta)=h_0(\eta),\;\theta(\eta)=\theta_0(\eta),\;\phi(\eta)=\;\phi_0(\eta)$$
$$f(\eta,\tau)=\;f_0(\eta)+\;e^{-\varepsilon\tau}F(\eta)$$
$$h(\eta,\tau)=\;h_0(\eta)+\;e^{-\varepsilon\tau}H(\eta)$$
$$\theta(\eta,\tau)=\;\theta_0(\eta)+\;e^{-\varepsilon\tau}G(\eta)$$
$$\phi(\eta,\tau)=\;\phi_0(\eta)+\;e^{-\varepsilon\tau}S(\eta) \tag{26}$$

Where the smallest eigenvalue is ε and $F(\eta)$, $H(\eta,$ $G(\eta),$ $S(\eta)$ are small relative to $f_0(\eta),$ $h_0(\eta),$ $\theta_0(\eta),$ $\phi_0(\eta)$ respectively. Equation (26) is used to create the linearized eigenvalue equations for equations (21) – (24), which generate the following:

$$(1+K)F_0'''+KH_0'-\left(\frac{2}{(m+1)}\right)F_0'\,[M-\varepsilon-2mf_0']+\left(\frac{2}{(m+1)}\right)[GrG_0+Gc\,S_0]+f_0F_0''+Ff_0''=0 \tag{27}$$

$$\left(1+\frac{K}{2}\right)H_0''-\frac{2}{(m+1)}H_0(2K-\varepsilon)-\frac{2K}{(m+1)}F_0''+f_0H_0'+F_0h_0'-\left(\frac{3m-1}{m+1}\right)[H_0f_0'+h_0F_0']=0 \tag{28}$$

$$\frac{1}{Pr}\left(1+\frac{4}{3}Rd\right)G_0''+\theta_0'[Nb\,S_0'+Nt\,2G_0'+F_0]+G_0'[Nb\,\phi_0'+f_0]+\left(\frac{2}{(m+1)}\right)\varepsilon G_0-Df\,S_0''=0 \tag{29}$$

$$S_0''+G_0''\left[\frac{Nt}{Nb}+Sr\,Sc\right]+\left(\frac{2}{(m+1)}\right)Sc\,\varepsilon S_0+\phi_0'F_0+S_0'f_0=0 \tag{30}$$

With boundary conditions:

$$F_0(0)=0,F_0'(0)=0,\;H_0(0)=-nF_0''(0),\;G_0(0)=0,\;S_0(0)=\;\;0$$
$$F_0(\eta)\rightarrow 0\,,H_0(\eta)\rightarrow 0\,,G_0(0)\rightarrow 0\,,S_0(0)\rightarrow 0 \qquad as\;\eta\rightarrow\infty \tag{31}$$

As stated by Harris et al. [24], variables $H_0'=1$ is used in place of the boundary conditions $H_0(\eta)\rightarrow 0$ as $\eta\rightarrow\infty$ to make sure that the least nonzero eigenvalues are produced accordingly.

4. Results and discussions

The effects of thermal radiation, Soret and Dufour on magnetohydrodynamics micropolar nanofluid flow over a non-linear vertical stretching/shrinking surface have been examined in this study. The governing equations of micropolar nanofluid flow (8) – (11), according to the boundary conditions (12), are numerically solved to investigate the flow and heat transfer properties. The outcomes of various flow properties are analyzed and illustrated with graphs. Table 1 presents a comparison between the current results and those obtained by

Hayat et al. [25]. It has been discovered that the current results are reliable and precise. Additionally, triple solutions are found in the micropolar nanofluid flow problem of all profiles, according to the computational results.

Table 2: Comparison of $(C_f(Re_x)^{\frac{1}{2}})$ for several of K and $n = 0, 0.5$ for $\lambda = 1$.

	$n = 0$		$n = 0.5$	
K	Hayat et al., [25]	Present	Hayat et al., [25]	Present
0	−1.00000	-1.00000	−1.00000	-1.00000
1	−1.367870	-1.367870	−1.224739	-1.224739
2	−1.621222	-1.621222	−1.414214	-1.414214
4	−2.004129	-2.004129	−1.732047	-1.732047

Stability analysis was conducted in this research work because to the presence of multiple solutions. Equations (27)-(30) have a minimal eigenvalue, which is concluded using the bvp4c MATLAB solver. In view of Lund et al., [26] state that an unstable flow with an initial development of disturbance is implied by a negative lowest eigenvalue, whereas a positive smallest eigenvalue denotes a stable flow with an initial decrease of disturbance. The first solution is found to have $\boldsymbol{\varepsilon > 0}$, but the second and third solutions have $\boldsymbol{\varepsilon < 0}$, according to the data shown in Table 3. As a result, it can be said that the first solution to this problem is both physically significant and stable. As a result, the decisions taken in this part will be dependent on the outcomes of the initial solution. However, there is still mathematical significance in the second and third answers.

Table 3. Various values of K and S for smallest eigenvalue.ε

K	S	1st Solution	2nd Solution	3rd Solution
0	3	0.45222	-1.03491	-1.03212
0	2.5	0.37321	-0.67641	-0.65741
0	2	0.02526	-0.11150	-0.11340
1	3	0.37826	-0.76105	-0.65104
1	2.5	0.12261	-0.44501	-0.29670
2	3	0.24073	-0.49360	-0.42360

Figure 2 shows the triple solutions of the velocity distribution for different values of M. It is essential that these triple solutions fulfill the boundary conditions. In the first solution, the velocity drops as the magnetic field increases due to a rise in Lorentz force. On the basis of science, the Lorentz force's produces a high resistance is the reason for a decrease in the momentum boundary layer thickness. In the second and third solutions, the dimensionless velocity rises as the magnetic field's effect increases.

Figure 3 shows the variations in the velocity profile for different values of n. The investigation indicates that in first, second and third solutions, when the variable n grows, the boundary layer and the micropolar nanofluid flow velocity both increases.

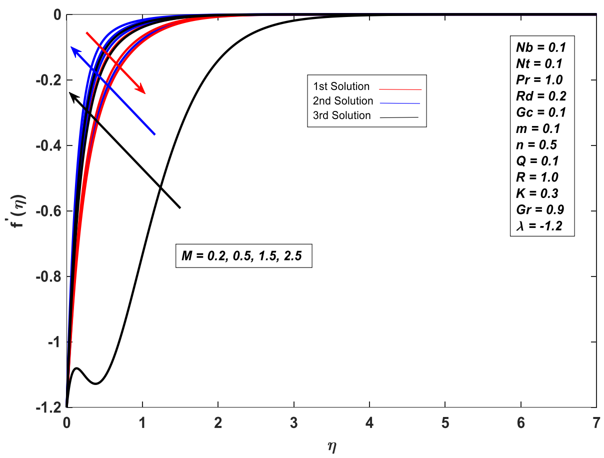

Figure 2: Velocity profile variations for various *M* values.

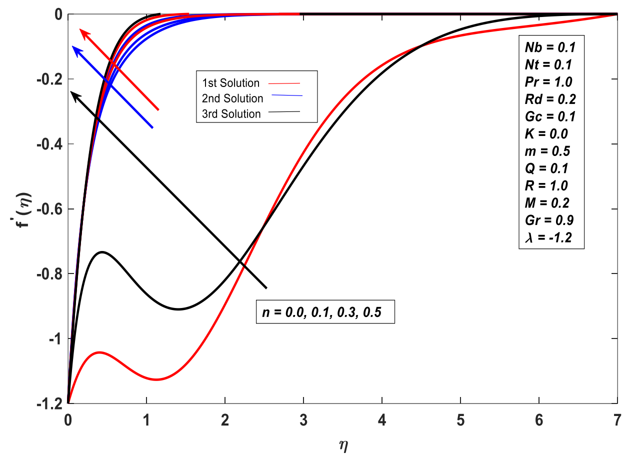

Figure 3: Velocity profile variations for various *n* values.

Figure 4 displays various values of buoyancy parameter Gr on the behaviour of velocity profile. The ratio of buoyancy to viscous forces in the movement of fluid is expressed by the buoyancy variable Gr. The velocity profile in the micropolar nanofluids gets improved by rise in the buoyancy variable Gr, according to three solutions. While Figure 5 demonstrates the effect of micropolar material factor K on the microrotation profile. When the numerical value of the micropolar material factor K grow in the first solution, the dimensionless microrotation profile and microrotation boundary layer are reduced. As K gets higher in the second and third solutions, the boundary layer and microrotation profile increases.

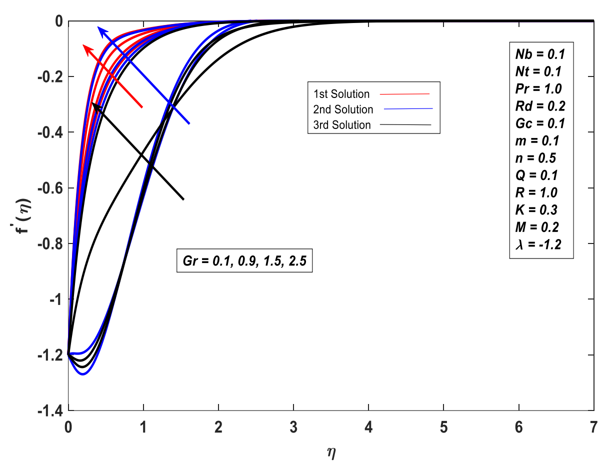

Figure 4: Velocity profile variations for various *Gr* values.

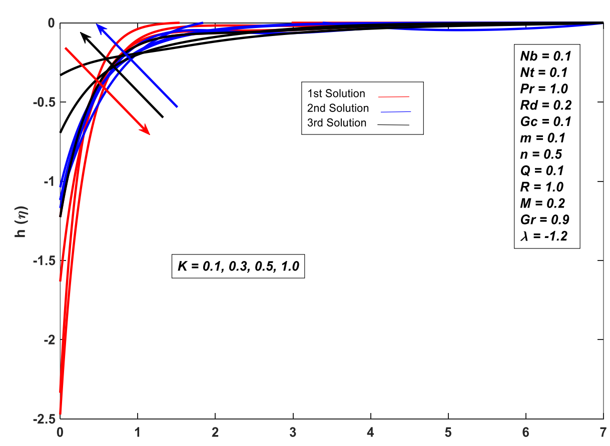

Figure 5: Microrotation profile variations for various *K* values.

Figure 6 indicates the impact of different values of thermal radiation Rd on temperature profile. The rate of heat transfer and the thermal boundary layer are decreased on temperature profile in the first, second and third solutions by increasing the thermal radiation. Figure 7 shows how the effect of Brownian motion factor Nb on temperature distribution. It is observed that as the Brownian motion factor Nb increases, the temperature of the micropolar nanofluid decreases consistently across first, second and third solutions.

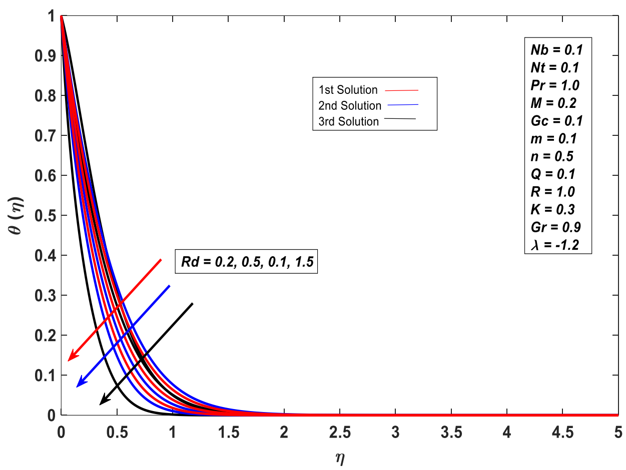

Figure 6: Temperature profile variations for various Rd values.

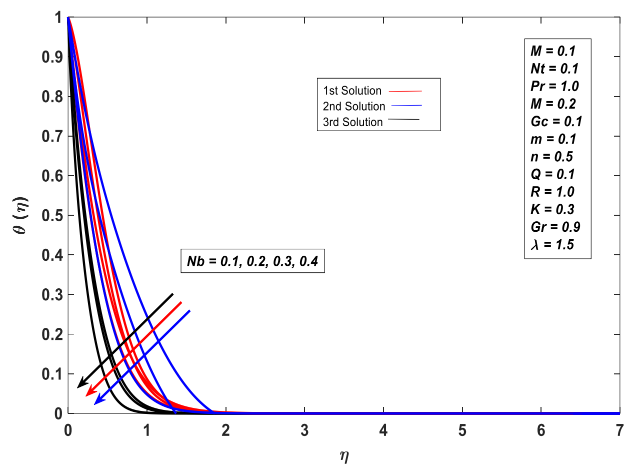

Figure 7: Temperature profile variations for various Nb values.

Figure 8 illustrates the influence of the thermophoresis factor Nt on temperature distribution. It is clear from every result that the temperature distribution and the thermal boundary layer thickness both rise with an increase in the thermophoresis factor Nt. Figure 9 represents the behaviour of the temperature distribution for various values of the Prandtl number Pr. The first, second and third solutions indicate that increasing Pr reduces the temperature profile, leading to a thinner thermal boundary layer.

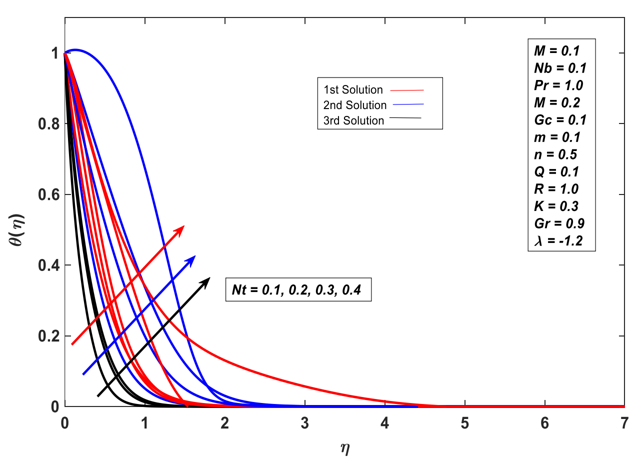

Figure 8: Temperature profile variations for various Nt values.

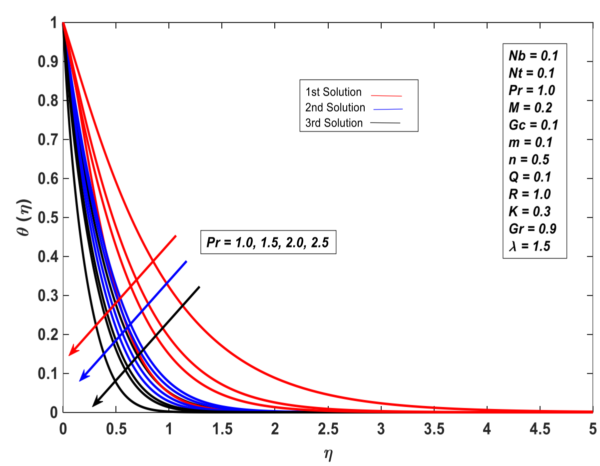

Figure 9: Temperature profile variations for various Pr values.

Figure 10 illustrates how Brownian motion impacts concentration profiles. It is clear from the first, second, and third solutions that the concentration profile and the boundary layer thickness drop with a rise in the Brownian motion factor Nb. Figure 11 indicates how the concentration profile is affected by the thermophoresis factor. When the thermophoresis factor Nt is increased, the concentration profile expands, along with an increase in its boundary thickness across all solutions.

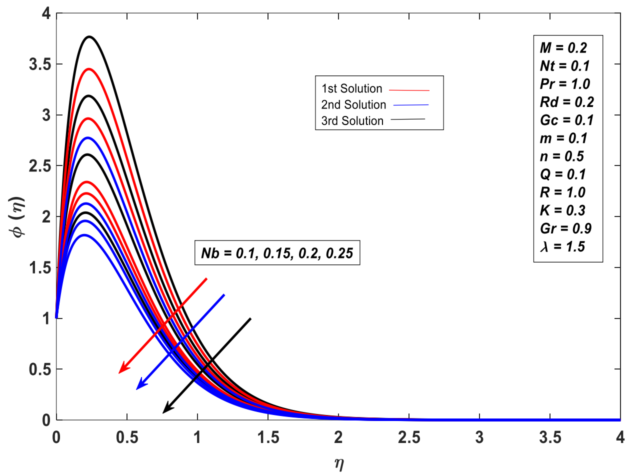

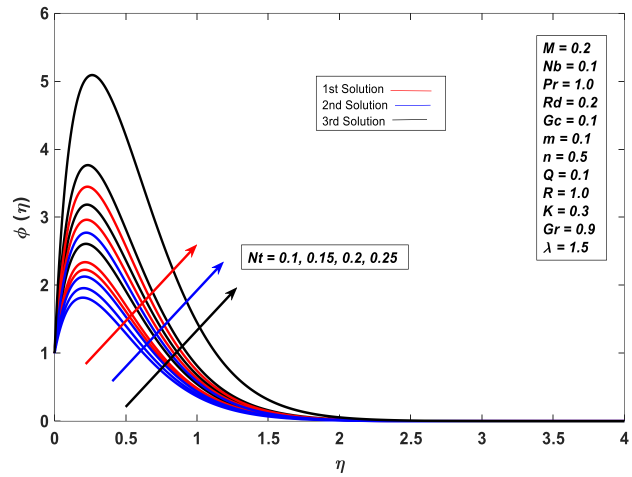

Fig. 10: Concentration profile variations for various Nb values **Fig. 11: Concentration profile variations for various Nt values**

Figure 12 illustrates that the temperature profile with increasing Dufour factor Df values. It shows a rise in the Dufour factor enhanced the temperature profile in each solution, which increased the rate at which mass diffusion proceeded. The temperature profile rises as a result of the enhanced mass diffusion-induced more effective energy transfer. Therefore, when Df values increase, the temperature profile gets more apparent. Figure 13 shows the impact of the Soret number Sr on the concentration profile. It shows that in first, second and third solutions, a rise in the Soret number corresponds to a rise in the concentration distribution. As a result, the Soret number rises, the concentration profile becomes clearer.

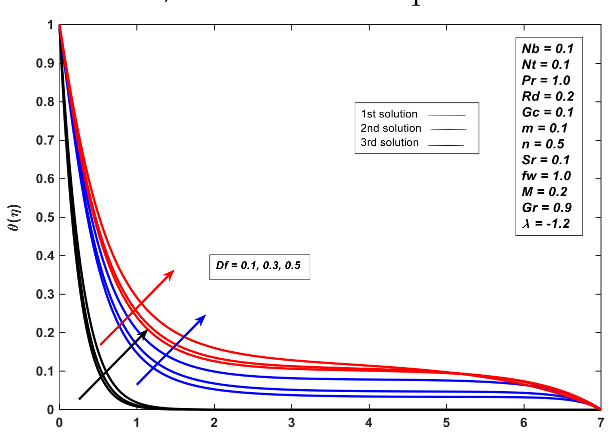

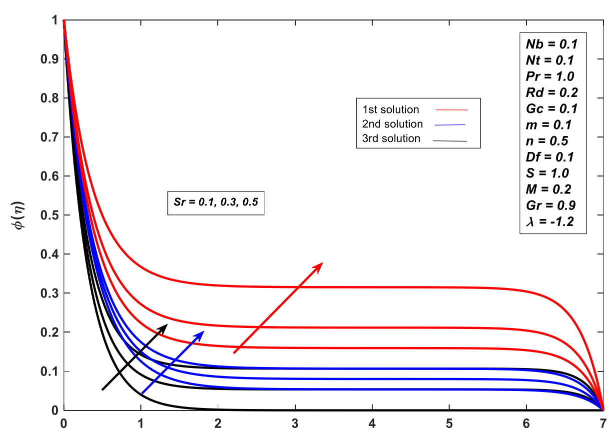

Fig 12: Temperature profile variations for various Df values. **Fig 13: Concentration profile variations for various Sr values**

Conclusion

In the current research, a numerical analysis is conducted on the magnetohydrodynamics flow of micropolar nanofluid over a vertical stretching/shrinking surface with the impacts of Soret and Dufour factors. The computational task is done by employing the bvp4c solver. The accuracy of the results is verified by the already published literature. In this investigation it is revealed that increasing the Soret effect raises the temperature of the nanoparticles near the vertical surface.

These are the main conclusions of this research:

1. The velocity distribution of the liquid shows decreasing behavior with the growth of the magnetic effect.
2. The concentration of nanoparticles decreases as N_b rises, and the concentration profile increases as N_t grows.
3. Temperature profile increases in the first, second and third solutions by increasing the impact of the Dufour number Df.
4. Concentration distribution increases in each solution by growing the impact of the Soret number Sr.

Acknowledgement: The author extends his appreciation to the Arab Open University for funding this work through AOU research fund No. (AOUKSA-524008).

Conflicts of Interest: The authors declare that there are no conflicts of interest regarding the publication of this paper.

References

[1] S.U.S. Choi, J.A. Eastman, Enhancing Thermal Conductivity of Fluids with Nanoparticles, in: International Mechanical Engineering Congress and Exhibition, San Francisco, CA, 1995. https://www.osti.gov/biblio/196525.

[2] A. Bouchireb, I. Khan, M. Kezzar, S. Alqahtani, M.R. Sari, K. Rafique, I. Tabet, Mhd Flow of Hybrid Nanofluid Between Convergent/divergent Channel by Using Daftardar-Jafari Method, BioNanoScience 14 (2024), 1583-1600. https://doi.org/10.1007/s12668-024-01401-4.

[3] K. Rafique, I. Khan, N.A. Mohammed, S. Alqahtani, T.A. Assiri, Keller Box Numerical Analysis of Power-Law Rotating Disk for Nanofluid Flow with Chemical Reaction, Numer. Heat Transfer, Part A: Appl. (2024), 1–18. https://doi.org/10.1080/10407782.2024.2338263.

[4] A. Refaie Ali, K. Rafique, M. Imtiaz, R. Jan, H. Alotaibi, I. Mekawy, Exploring Magnetic and Thermal Effects on Mhd Bio-Viscosity Flow at the Lower Stagnation Point of a Solid Sphere Using Keller Box Technique, Partial. Differ. Equ. Appl. Math. 9 (2024), 100601. https://doi.org/10.1016/j.padiff.2023.100601.

[5] H. Alotaibi, K. Rafique, Numerical Simulation of Nanofluid Flow Between Two Parallel Disks Using 3-Stage Lobatto III-A Formula, Open Phys. 20 (2022), 649-656. https://doi.org/10.1515/phys-2022-0059.

[6] B. Lemouedda, M. Kezzar, K. Rafique, M.R. Sari, I. Tabet, I. Khan, Ternary Nanoparticles Effect in Rotating Hydromagnetic Jeffery-Hamel Flow of Nanofluids, Proc. Inst. Mech. Eng. Part N: J. Nanomater. Nanoeng. Nanosyst. (2024). https://doi.org/10.1177/23977914241261514.

[7] K. Cacua, R. Buitrago-Sierra, E. Pabón, A. Gallego, C. Zapata, B. Herrera, Nanofluids Stability Effect on a Thermosyphon Thermal Performance, Int. J. Therm. Sci. 153 (2020), 106347. https://doi.org/10.1016/j.ijthermalsci.2020.106347.

[8] A. Faqih, F.M. Rafique, K. Aslam, M.Z. Swalmeh, Numerical Analysis on Stagnation Point Flow of Micropolar Nanofluid with Thermal Radiations over an Exponentially Stretching Surface, WSEAS Trans. Fluid Mech. 19 (2024), 40-48.

[9] P. Durga Prasad, R. Kiran Kumar, S. Varma, Heat and Mass Transfer Analysis for the Mhd Flow of Nanofluid with Radiation Absorption, Ain Shams Eng. J. 9 (2018), 801-813. https://doi.org/10.1016/j.asej.2016.04.016.

[10] R.P. Sharma, S.R. Mishra, S. Tinker, Influence of Soret and Dufour Effect on MHD Flow over an Exponential Stretching Sheet: A Numerical Study, Indian J. Pure Appl. Phys. 58 (2020), 558-568.

[11] R.G. Srinivasa, B. Ramana, R.B. Reddy, G. Vidyasagar, Soret and Dufour Effects on MHD Boundary Layer Flow over a Moving Vertical Porous Plate with Suction, Int. J. Emerg. Trends Eng. Dev. 2 (2014), 215-226.

[12] N. Vedavathi, K. Ramakrishna, K. Jayarami Reddy, Radiation and Mass Transfer Effects on Unsteady Mhd Convective Flow Past an Infinite Vertical Plate with Dufour and Soret Effects, Ain Shams Eng. J. 6 (2015), 363-371. https://doi.org/10.1016/j.asej.2014.09.009.

[13] G. Rasool, A. Shafiq, D. Baleanu, Consequences of Soret–dufour Effects, Thermal Radiation, and Binary Chemical Reaction on Darcy Forchheimer Flow of Nanofluids, Symmetry 12 (2020), 1421. https://doi.org/10.3390/sym12091421.

[14] D. Pal, G. Mandal, K. Vajravalu, Soret and Dufour Effects on Mhd Convective–radiative Heat and Mass Transfer of Nanofluids Over a Vertical Non-Linear Stretching/shrinking Sheet, Appl. Math. Comput. 287-288 (2016), 184-200. https://doi.org/10.1016/j.amc.2016.04.037.

[15] K. Rafique, M.I. Anwar, M. Misiran, M.I. Asjad, Energy and Mass Transport of Micropolar Nanofluid Flow Over an Inclined Surface with Keller-box Simulation, Heat Transf. 49 (2020), 4592-4611. https://doi.org/10.1002/htj.21843.

[16] M.A. Kumar, Y.D. Reddy, B.S. Goud, V.S. Rao, Effects of Soret, Dufour, Hall Current and Rotation on Mhd Natural Convective Heat and Mass Transfer Flow Past an Accelerated Vertical Plate Through a Porous Medium, Int. J. Thermofluids 9 (2021), 100061. https://doi.org/10.1016/j.ijft.2020.100061.

[17] H. ALFVÉN, Existence of Electromagnetic-Hydrodynamic Waves, Nature 150 (1942), 405-406. https://doi.org/10.1038/150405d0.

[18] N.A. Zainal, R. Nazar, K. Naganthran, I. Pop, Unsteady Mhd Mixed Convection Flow in Hybrid Nanofluid at Three-Dimensional Stagnation Point, Mathematics 9 (2021), 549. https://doi.org/10.3390/math9050549.

[19] A. Ishak, R. Nazar, I. Pop, Magnetohydrodynamic (MHD) Flow of a Micropolar Fluid Towards a Stagnation Point on a Vertical Surface, Comput. Math. Appl. 56 (2008), 3188-3194. https://doi.org/10.1016/j.camwa.2008.09.013.

[20] M.G. Reddy, N.B. Reddy, Mass Transfer and Heat Generation Effects on Mhd Free Convection Flow Past an Inclined Vertical Surface in a Porous Medium, J. Appl. Fluid Mech. 4 (2011), 7-11. https://doi.org/10.36884/jafm.4.02.11911.

[21] S. Baag, S. Mishra, G. Dash, M. Acharya, Numerical Investigation on Mhd Micropolar Fluid Flow Toward a Stagnation Point on a Vertical Surface with Heat Source and Chemical Reaction, J. King Saud Univ. - Eng. Sci. 29 (2017), 75-83. https://doi.org/10.1016/j.jksues.2014.06.002.

[22] W. Khan, I. Pop, Boundary-layer Flow of a Nanofluid Past a Stretching Sheet, Int. J. Heat Mass Transfer 53 (2010), 2477-2483. https://doi.org/10.1016/j.ijheatmasstransfer.2010.01.032.

[23] E. Seid, E. Haile, T. Walelign, Multiple Slip, Soret and Dufour Effects in Fluid Flow Near a Vertical Stretching Sheet in the Presence of Magnetic Nanoparticles, Int. J. Thermofluids 13 (2022), 100136. https://doi.org/10.1016/j.ijft.2022.100136.

[24] P. Orsini, H. Power, M. Lees, H. Morvan, A Control Volume Radial Basis Function Techniques for the Numerical Simulation of Saturated Flows in Semi-Confined Aquifer, Transp. Porous Media 79 (2008), 171-196. https://doi.org/10.1007/s11242-008-9304-y.

[25] T. Hayat, M.I. Khan, M. Waqas, A. Alsaedi, M.I. Khan, Radiative Flow of Micropolar Nanofluid Accounting Thermophoresis and Brownian Moment, Int. J. Hydrog. Energy 42 (2017), 16821-16833. https://doi.org/10.1016/j.ijhydene.2017.05.006.

[26] L.A. Lund, Z. Omar, I. Khan, Quadruple Solutions of Mixed Convection Flow of Magnetohydrodynamic Nanofluid Over Exponentially Vertical Shrinking and Stretching Surfaces: Stability Analysis, Comput. Methods Programs Biomed. 182 (2019), 105044. https://doi.org/10.1016/j.cmpb.2019.105044.

[27] L.A. Lund, Z. Omar, I. Khan, S. Dero, Multiple Solutions of Cu-$C_6H_9NaO_7$ and Ag- $C_6H_9NaO_7$ Nanofluids Flow Over Nonlinear Shrinking Surface, J. Cent. South Univ. 26 (2019), 1283-1293. https://doi.org/10.1007/s11771-019-4087-6.